LETTERS

Charge- and size-based separation of macromolecules using ultrathin silicon membranes

Christopher C. Striemer[1], Thomas R. Gaborski[2], James L. McGrath[2] & Philippe M. Fauchet[1]

Commercial ultrafiltration and dialysis membranes have broad pore size distributions and are over 1,000 times thicker than the molecules they are designed to separate, leading to poor size cut-off properties, filtrate loss within the membranes, and low transport rates[1,2]. Nanofabricated membranes have great potential in molecular separation applications by offering more precise structural control[3,4], yet transport is also limited by micrometre-scale thicknesses[5]. This limitation can be addressed by a new class of ultrathin nanostructured membranes where the membrane is roughly as thick (~10 nm) as the molecules being separated, but membrane fragility and complex fabrication have prevented the use of ultrathin membranes for molecular separations[1]. Here we report the development of an ultrathin porous nanocrystalline silicon (pnc-Si) membrane using straightforward silicon fabrication techniques that provide control over average pore sizes from approximately 5 nm to 25 nm. Our pnc-Si membranes can retain proteins while permitting the transport of small molecules at rates an order of magnitude faster than existing materials, separate differently sized proteins under physiological conditions, and separate similarly sized molecules carrying different charges. Despite being only 15 nm thick, pnc-Si membranes that are free-standing over 40,000 μm^2 can support a full atmosphere of differential pressure without plastic deformation or fracture. By providing efficient, low-loss macromolecule separations, pnc-Si membranes are expected to enable a variety of new devices, including membrane-based chromatography systems and both analytical and preparative microfluidic systems that require highly efficient separations.

Given the potential of nanofabricated membranes to advance macromolecular separation processes and the limitations of existing materials, we have developed a robust and inexpensive ultrathin porous membrane. Our fabrication process is shown schematically in Fig. 1a, and is described in detail in the Methods section. Briefly, our approach uses precision silicon deposition and etching techniques to create the ultrathin membrane. However, instead of directly patterning pores, we have discovered that voids are formed spontaneously as nanocrystals nucleate and grow in a 15-nm-thick amorphous silicon (a-Si) film during a rapid thermal annealing step. The voids span the molecularly thin membrane to create pores. The resulting membranes cover openings several hundred micrometres across in a rigid crystalline silicon frame, and can therefore be easily handled and used.

Figure 1b shows a plan-view transmission electron microscopy (TEM) image of a 15-nm-thick pnc-Si membrane. In this image, the pores appear as white circles while the solid nanocrystalline silicon is grey and black owing to electron diffraction. Nanocrystals with aligned atomic planes that satisfy the Bragg condition for the electron beam cause strong diffraction, and make the nanocrystals appear black in the bright field image. Nanocrystals not satisfying the Bragg condition appear grey. All structures visible in this image were formed during a single 30 s anneal at 770 °C, yielding well defined pores with diameters of 9–35 nm.

In addition to TEM, several other characterization techniques have been used to confirm the properties of our pnc-Si membranes. Figure 2a shows refractive index dispersion data obtained using spectroscopic ellipsometry for a 15-nm-thick silicon film after deposition

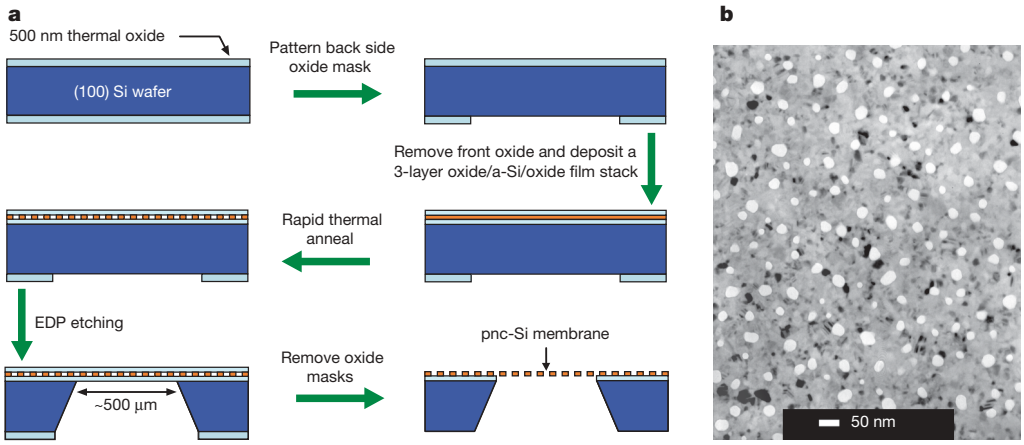

Figure 1 | Fabrication and pore morphology of pnc-Si membrane. **a**, Standard microfabrication tools are used to deposit, pattern and suspend pnc-Si films. **b**, A plan-view TEM image of the porous nanostructure of a 15-nm-thick membrane. In this bright field image, pores appear as bright spots while nanocrystalline silicon is in grey or black contrast.

[1]Department of Electrical and Computer Engineering, University of Rochester, Rochester, New York 14627, USA. [2]Department of Biomedical Engineering, University of Rochester, Rochester, New York 14620, USA.

(a-Si) and after crystallization (pnc-Si). Our sputtered a-Si has high optical density, comparable to microelectronic quality a-Si deposited with chemical vapour deposition, and exhibits a clear shift in optical properties after crystallization, with characteristic resonance peaks similar to crystalline silicon[6]. These data are indicative of high purity silicon films with smooth interfaces. It should also be noted that TEM images of the as-deposited a-Si show no distinguishable voids or crystalline features. To confirm the accuracy of our spectroscopic ellipsometry data, several membranes were transferred onto polished quartz and atomic force microscopy (AFM) was used to measure the step height of the membrane edge. Figure 2b shows an AFM image that confirms the 15 nm thickness of a sample membrane and its highly smooth surface morphology.

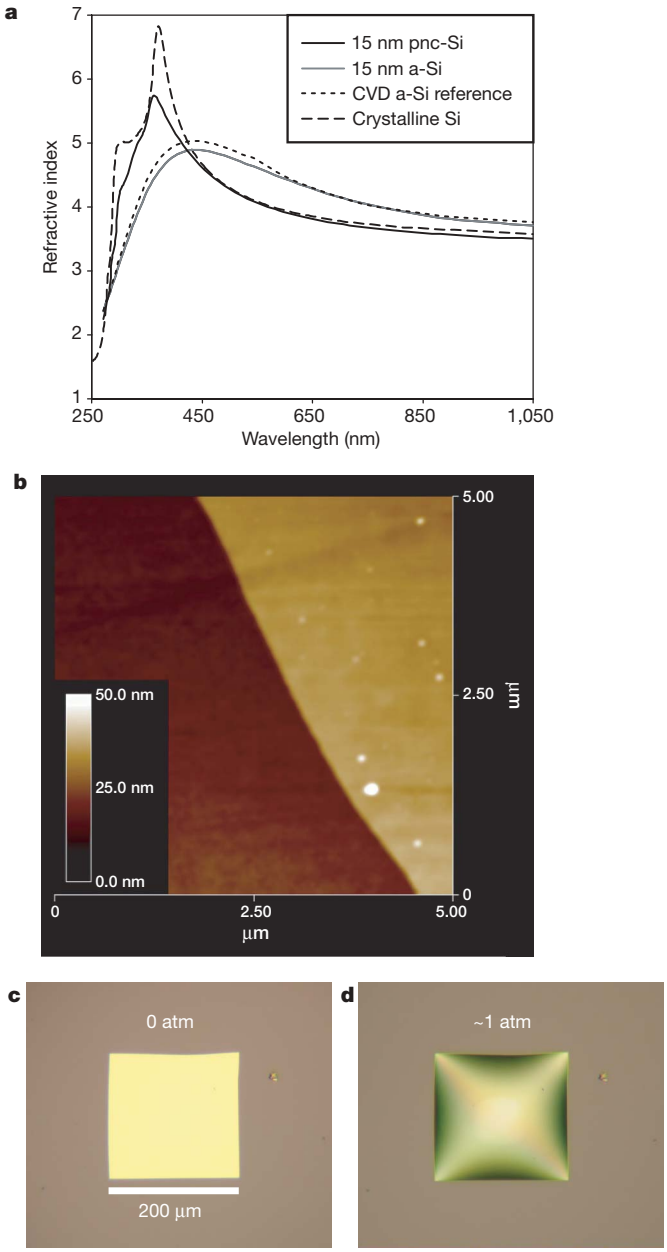

Figure 2 | Physical properties of pnc-Si membranes. a, Refractive index dispersion curves of our high optical density silicon film before and after crystallization (729 °C, 30 s anneal), determined by spectroscopic ellipsometry. Dispersion curves for crystalline silicon and a-Si grown by chemical vapour deposition (CVD) are also plotted for reference. **b**, An AFM scan over the edge of a membrane transferred to a polished quartz window confirms 15 nm thickness and minimal roughness. **c**, **d**, Optical micrographs of a 15-nm-thick pnc-Si membrane at equilibrium (**c**) and with ~1 atm (15 p.s.i.) of back pressure (**d**), demonstrating the remarkable strength of this ultrathin material.

Another important characteristic of pnc-Si membranes is their remarkable mechanical stability. We mechanically tested membranes using a customized holder to apply pressure to one side of the membrane while an optical microscope was used to monitor deformation. Figure 2c, d shows optical micrographs of a 200 μm × 200 μm × 15 nm membrane as more than 1 atm of differential pressure was applied across it for approximately 5 min. With no differential pressure, the membrane is extremely flat (Fig. 2c), and at maximum pressure (Fig. 2d) the membrane elastically deforms but maintains its structural integrity throughout the duration of test. Unlike thin polymer membranes[7], pnc-Si membranes exhibit no plastic deformation and immediately return to their flat state when the pressure is removed. Pressurization tests were cycled three times with no observable membrane degradation. The remarkable strength and durability exhibited by these membranes is likely to be due to their smooth surfaces[1] and random nanocrystal orientation that inhibit the formation and propagation of cracks.

We have also determined that pore size distributions in pnc-Si membranes can be controlled through adjustment of the rapid thermal annealing temperature during crystallization. Nanocrystal nucleation and growth are Arrhenius-like processes[8] that exhibit strong temperature dependence above a threshold crystallization temperature of approximately 700 °C in a-Si (ref. 9). Existing crystallization models[10] fail to predict void formation, and must be extended to account for how volume contraction and material strain lead to pore formation in ultrathin membranes. To demonstrate pore size tunability, three wafers with 15-nm-thick pnc-Si membranes were processed identically, except for the annealing temperature. TEM images of these membranes (Fig. 3, right) revealed that pore size and density increase monotonically with temperature, as samples annealed at 715 °C, 729 °C and 753 °C have average pore sizes of 7.3 nm, 13.9 nm and 21.3 nm, respectively. A sample annealed at 700 °C exhibited no crystallinity or voids, illustrating a strong morphological dependence on temperature near the onset of crystallization. The tunability of pore size in this range makes pnc-Si membranes particularly well suited for size-selective separation of large biomolecules, such as proteins and DNA. Because pore area is central to the discussion of molecular transport through these membranes, histograms that identify the total pore area available at each pore size are presented in Fig. 3, left. Pore size data were extracted directly from the micrographs using image processing software.

To demonstrate molecular separations with pnc-Si, we chose two common blood proteins of different molecular weight (MW) and hydrodynamic diameter (D); bovine serum albumin, BSA (MW = 67,000 (67K), $D = 6.8$ nm) and immunoglobulin-γ, IgG (MW = 150K, $D = 14$ nm), fluorescently labelled with Alexa 488 and Alexa 546 (Molecular Probes), respectively. Free Alexa 546 dye was used as an additional low molecular weight (MW = 1K, $D \approx 1$ nm) species. We monitored the passage of these species through the pnc-Si membranes shown in Fig. 3 using real time fluorescence microscopy (Fig. 4a). In this set-up, a membrane and its supporting silicon wafer frame was placed above a glass slide with 50 μm silica bead spacers, forming a thin diffusion chamber beneath the membrane. The chamber was first filled with approximately 50 μl of clean buffer solution and then 3 μl of a fluorescent mixture was added to the well above the membrane. An image of the membrane edge was taken every 30 s in each of the fluorescence channels. The passage of each species through the membrane was observed as the spreading of fluorescence signal from the membrane edge, as illustrated in the two false-colour images in Fig. 4a.

Figure 4b shows quantitative results for the separation of free Alexa 546 dye and BSA using membrane A (Fig. 3a). These data were generated by plotting the fluorescence intensity at a point 50 μm away from the membrane edge for a time series of images. From these results, it is clear that dye passes freely through the membrane while

BSA is almost completely blocked. Figure 4c shows a similar experiment, where the permeabilities of IgG and BSA through membrane B at 1 μM concentration are compared. In this case, BSA diffuses through the membrane >4 times more rapidly than IgG. Because the diffusion coefficients for these molecules are within 25% of each other[11], the rate difference that we measure clearly indicates that pnc-Si membranes hinder IgG diffusion relative to BSA diffusion. By more thoroughly optimizing pore sizes, we expect to engineer pnc-Si membranes that can completely exclude IgG but permit BSA passage. The plots of Fig. 4b and c can be quantitatively compared for BSA, demonstrating that the increased cut-off size of membrane B allows a 15 times enhancement of BSA diffusion relative to membrane A. Time-lapse movies of these two separation experiments are included in Supplementary Information.

An interesting finding from our separation experiments was that BSA and IgG are retained behind membranes with maximal pore sizes more than twice as large as their reported hydrodynamic diameters. As a potential explanation, we investigated the possibility that electrostatic interactions and protein adsorption might create an effective pore size smaller than that measured by TEM. Indeed, the passage of negatively charged Alexa 488 (2−) dye in the presence and absence of high salt concentrations suggests a role for electrostatic interactions in determining effective pore sizes. As shown in Fig. 4d, the transport of the Alexa dye drops by a factor of 10 when experiments are conducted in deionized water. We interpret this as a consequence of electrostatic repulsion between the dye and a negatively charged native oxide layer on the surface of the pnc-Si membranes.

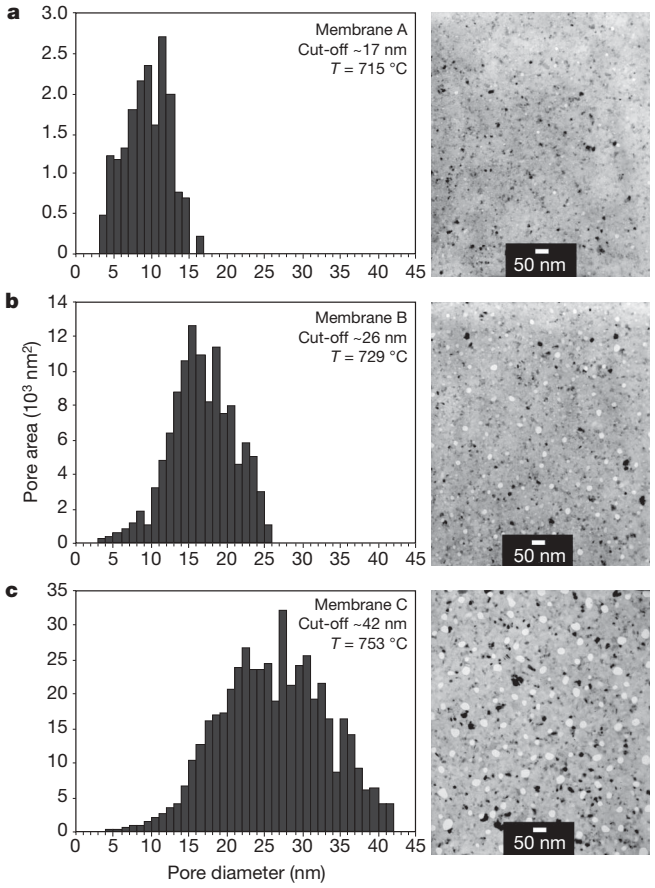

Figure 3 | Tunability of pnc-Si membrane pore size for molecular separation experiments. By varying the temperature at which the silicon film is crystallized, pore diameter can be controlled. The maximum (cut-off) pore size and porosity increase with annealing temperature from **a**, 715 °C to **b**, 729 °C and **c**, 753 °C, as illustrated in the histograms that plot total pore area available for molecular transport at each pore diameter. The TEM image used to generate each histogram is included on the right side.

Consistent with this interpretation, high salt concentrations increase throughput by screening surface and solute charges. To provide further evidence of charge effects, we modified membranes to carry abundant negative and positive surface charges. We found that in low ionic strength solutions, positively charged membranes blocked only positively charged dyes and negatively charged membranes blocked only negatively charged dyes (Supplementary Fig. S1). Although the high ionic strength of phosphate buffered saline should largely screen the charge of the native membrane oxide for our protein separations, proteins are much larger molecules and can be heavily charged (BSA net molecular charge is 13− at pH 7)[12], so stronger electrostatic interactions that reduce the effective pore size are expected. In addition to offering a partial explanation for reduced effective pore sizes in charge separations, these studies clearly demonstrate that pnc-Si membranes can be functionalized to separate similarly sized molecules on the basis of their charge.

Protein adsorption to the pore walls will also reduce effective pore size. By directly staining for protein on pnc-Si membranes used for separations, it is evident that BSA adsorption shrinks, but does not occlude, the largest membrane pores by as much as 7 nm (Supplementary Fig. S2). In addition to charge and adsorption effects, we expect other factors to reduce effective pore sizes, such as the uncertain relationship between a protein's physical size and hydrodynamic dimensions, and the behaviour of water (hydrogen bonding) in nanoscale pores.

Given the hours-long passage-times of molecules through thick membranes[3], it is significant that filtrate molecules appear downstream of pnc-Si filters within minutes. To better quantify the transport through pnc-Si membranes, we followed the fluorescence microscopy experiments with bench-top experiments in which we could remove and assay the Alexa 546 dye that diffused across membrane A from a 100 μM starting concentration using a similar unstirred geometry. We compared dye diffusion through pnc-Si membranes to diffusion through standard regenerated cellulose dialysis membranes (Spectra/Por 7 dialysis membrane, molecular-weight cut-off = 50K). The results shown in Fig. 4e reveal that dye diffuses over 9 times faster through pnc-Si membranes than dialysis membranes with comparable size exclusion properties (a 50K cut-off dialysis membrane was chosen, based on the excellent retention of BSA (67K) by membrane A in Fig. 4b). The pnc-Si membranes exhibit an initial transport rate of 156 nmol $cm^{-2} h^{-1}$ (Fig. 4e) that rapidly slows as the 3 μl source volume depletes, lowering the concentration gradient across the barrier. Remarkably, when this experiment was repeated with membrane C for 1 h, an increase of <10% in dye transport was measured relative to membrane A, despite porosities differing by ~29 times (0.2% versus 5.7%). We interpret this as evidence that dye or small molecule transport is essentially unhindered by our membranes, as porosities far lower than that of membrane A should theoretically allow greater than half-maximal diffusion through an infinitely thin porous barrier[13]. Therefore, the observed 9 times increase in diffusion rate over conventional dialysis membranes indicates that diffusion through the commercial membrane is the rate-limiting transport process, whereas diffusion through the bulk solution is rate-limiting for the pnc-Si membrane experiment. Substantial enhancement of transport rate is expected in systems that implement active mixing, or forced flow (pressure- or voltage-driven).

Our work with pnc-Si membranes represents the first use of ultrathin nanomembranes for size-based molecular separations, and encourages their use in several near-term applications. First, the separation of BSA and IgG suggests that pnc-Si can be used for membrane-based protein fractionation. BSA and IgG are too close in size (2.2 times MW difference) to be efficiently separated using conventional membrane processes[14] (>10 times MW difference is recommended by the manufacturers), and much of the filtrate species is lost to the high surface area and tortuous porosity of these standard membranes. By minimizing filter material, pnc-Si

membranes should allow for recovery of both the retentate and filtrate fractions to enable membrane-based chromatography. Second, because they are molecularly thin and have a minimal filter surface area, pnc-Si membranes are expected to be highly efficient for separation processes. Indeed, our diffusion measurements recorded a transport rate of 156 nmol cm^{-2} h^{-1} for Alexa 546 dye. This rate is more than one order of magnitude faster than those for thick nanofabricated membranes[3], and >9 times faster than our own measurements through dialysis membranes. We further demonstrated that pnc-Si membranes with fixed charges can be used to separate similarly sized molecules with different charges, adding another dimension of control for highly efficient molecular separations[15]. Finally, the silicon-based platform opens several avenues for future developments, including scalable production of membranes, straightforward integration into microfluidic devices, and surface functionalization using well-established chemistries[16,17] to modify surface charge, reduce protein adsorption and protect the silicon from chemical attack in harsh environments. Importantly, the demonstrated

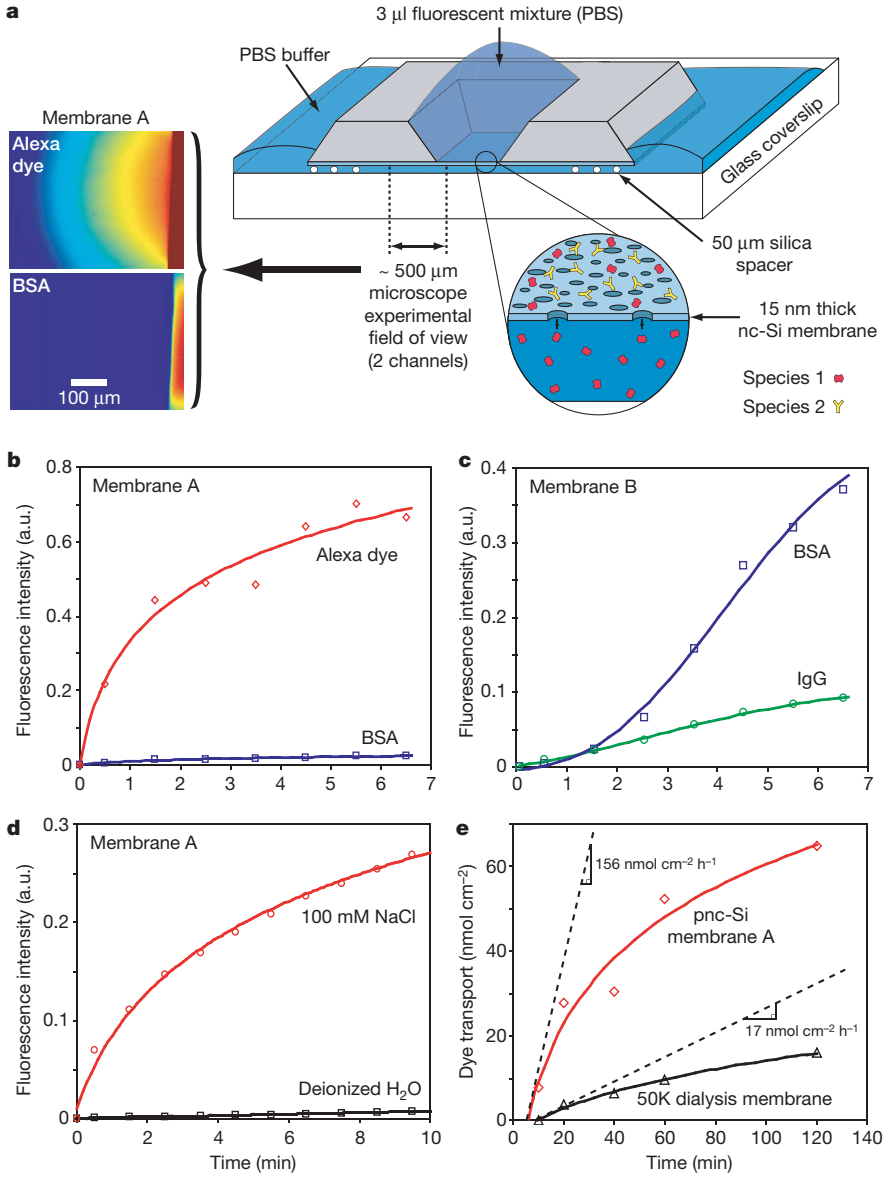

Figure 4 | Molecular separation and transport rates through pnc-Si membranes. **a**, The passage of two fluorescent species (labelled proteins or free dye) from a 3 µl source mixture through pnc-Si membranes was monitored simultaneously on two channels of a fluorescence microscope. The membrane edge was imaged from below and the lateral spread of fluorescent material was monitored to determine permeation through the membrane. Experimental false-colour images of the two fluorescence channels taken 6.5 min after the application of a mixture of labelled BSA (MW = 67K) and free Alexa 546 dye (MW = 1K) clearly show species separation. The membrane edge is the bright feature on the right side of each image, corresponding to the fluorescence generated in the source solution behind the membrane. Spread of the fluorescence signal beyond the membrane edge quantitatively indicates transport through the membrane. **b**, As shown in **a**, highly efficient separation of BSA and free dye was observed through membrane A (Fig. 3a) over 6.5 min. A plot of the fluorescence intensity 50 µm from the membrane edge was generated from a time series of images. Intensities were normalized to the centre value of the membrane in the first frame for each channel. **c**, A greater than fourfold separation of proteins BSA and IgG (MW = 150K) was observed through membrane B (Fig. 3b) using the same method. **d**, The transport of dye through membrane A was determined for solutions with high and low ionic strength using the set-up from **a**. **e**, The diffusion rate of dye through membrane A was benchmarked relative to a commercial dialysis membrane with a 50K cut-off (50 times larger than the dye MW). Because the 3 µl of source dye quickly depletes, the transport rate is calculated as the initial slope of the transport curve. Dye concentration was measured by 558 nm absorption at each time point.

mechanical strength of these ultrathin membranes should allow the construction of large-scale dialysis systems, and facilitate their use in pressurized filtration devices at the macro- and microscale.

METHODS

Fabrication. The pnc-Si membranes are fabricated by the procedure outlined in Fig. 1. We first grow a 500-nm-thick layer of SiO_2 on both sides of a silicon wafer. On the back side of the wafer, the SiO_2 is patterned using standard photolithography techniques to form an etch mask for the membrane formation process. The front oxide layer is then removed, and a high quality three layer film stack (20 nm SiO_2 / 15 nm a-Si / 20 nm SiO_2) is deposited on the front surface using RF magnetron sputtering. The a-Si layer is sputtered at a chamber pressure of 1.5 mtorr in Ar with a target power density of 0.4 W cm^{-2}, yielding a deposition rate of 3.4 nm min^{-1}. The SiO_2 layers are reactively sputtered from a silicon target at a chamber pressure of 1.5 mtorr, with a (3:4) Ar:O_2 gas flow ratio, and a target power density of 1.8 W cm^{-2}, yielding a deposition rate of 10.7 nm min^{-1}. Our deposition recipe is well characterized, and we are able to deposit films with $\pm 1\%$ thickness accuracy and surface roughness <0.5 nm. We have previously demonstrated the crystallization of very thin amorphous silicon films, forming high quality nanocrystals with well-defined size[18].

To form the pnc-Si membranes, the substrate is briefly exposed to high temperature (715–770 °C for 30 s) in a rapid thermal processing chamber, crystallizing the a-Si into a nanocrystalline film. The patterned wafer back side is then exposed to a highly selective silicon etchant, EDP (ethylenediamine pyrocatechol)[19], which removes the silicon wafer along (111) crystal planes until it reaches the first SiO_2 layer of the front side film stack. This etch is also used to outline approximately 80 samples (3.5 mm × 9 mm) that can be easily removed from the wafer after the fabrication process is complete, and used individually for molecular separation experiments. Finally, exposing the three layer membrane to buffered oxide etchant removes the protective oxide layers, leaving only the freely suspended ultrathin pnc-Si membrane. We have used this process to fabricate square membranes as thin as 5 nm and as large as 2 mm × 2 mm, but in this Letter we focus on more structurally robust 15-nm-thick membranes, measuring several hundred micrometres per side.

Membrane processing. Silicon surfaces exposed to air tend to grow a native oxide that reaches a thickness of ~1 nm within a few hours and stabilizes at ~1.5 nm in approximately 1 week (characterized by us using spectroscopic ellipsometry). This process can be accelerated by exposure to an oxygen plasma at 450 °C and the oxide growth also self-limits at ~1.5 nm thickness under these conditions. The membranes used in Supplementary Fig. S1 were exposed to a 500 W RF oxygen plasma at 450 °C and 12 mtorr for 60 s to form a stable surface oxide. Silanization was then performed on several membranes after oxidation, using a recipe that we have used previously[17]. Briefly, the membranes were first cleaned in a 1:1 solution of HCl:methanol for 30 min. The samples were then soaked for 15 min in a solution of 1.5 ml 5% (aminopropyl)triethoxysilane (APTES) in deionized water added to 28.5 ml acetone. Membranes were then dried and baked for 15 min at 100 °C. This process forms a monolayer of APTES with a thickness of approximately 0.8 nm (ref. 20).

Protein separation. For the protein separation experiments, BSA and IgG were labelled with Alexa Fluor 488 and 546 dyes (Molecular Probes). The dyes react with primary amines, forming stable covalent bonds. Each species was twice purified with spin columns provided in the labelling kit. Protein concentration and degree of labelling was calculated by measuring absorbances with a spectrophotometer using extinction coefficients provided by the dye manufacturer. This analysis showed that BSA was labelled with eight moles of dye per mole of protein, while IgG was labelled with three moles of dye per mole of protein. In our microscope, this yielded similar fluorescence intensity for each species at the same concentration. In the protein separation experiments, proteins were used at 1 μM, while free dye was used at 100 μM to mimic the separation of proteins from higher concentration solute species, as might occur in buffer exchange or desalting applications. In the electrochemical double layer experiments, Alexa and Rhodamine 6G dyes were used at 50 μM. All plots and figures were normalized (as described in Fig. 4 legend) for comparative purposes.

Received 23 March; accepted 20 November 2006.

1. Tong, H. D. *et al.* Silicon nitride nanosieve membrane. *Nano Lett.* **4,** 283–287 (2004).
2. Kuiper, S., van Rijn, C. J. M., Nijdam, W. & Elwenspoek, M. C. Development and applications of very high flux microfiltration membranes. *J. Membr. Sci.* **150,** 1–8 (1998).
3. Yamaguchi, A. *et al.* Self-assembly of a silica-surfactant nanocomposite in a porous alumina membrane. *Nature Mater.* **3,** 337–341 (2004).
4. Lee, S. B. & Martin, C. R. Electromodulated molecular transport in gold-nanotubule membranes. *J. Am. Chem. Soc.* **124,** 11850–11851 (2002).
5. Martin, F. *et al.* Tailoring width of microfabricated nanochannels to solute size can be used to control diffusion kinetics. *J. Control. Release* **102,** 123–133 (2005).
6. Palik, E. D. *Handbook of Optical Constants of Solids* 547–569 (Academic, Orlando, 1985).
7. Jiang, C. *et al.* Freely suspended nanocomposite membranes as highly sensitive sensors. *Nature Mater.* **3,** 721–728 (2004).
8. Spinella, C., Lombardo, S. & Priolo, F. Crystal grain nucleation in amorphous silicon. *J. Appl. Phys.* **84,** 5383–5414 (1998).
9. Zacharias, M. *et al.* Thermal crystallization of amorphous Si/SiO_2 superlattices. *Appl. Phys. Lett.* **74,** 2614–2616 (1999).
10. Zacharias, M., Heitmann, J., Schmidt, M. & Streitenberger, P. Confinement effects in crystallization and Er doping of Si nanostructures. *Physica E* **11,** 245–251 (2001).
11. Karlsson, D., Zacchi, G. & Axelsson, A. Electronic speckle pattern interferometry: a tool for determining diffusion and partition coefficients for proteins in gels. *Biotechnol. Prog.* **18,** 423–430 (2002).
12. Pujar, N. S. & Zydney, A. L. Electrostatic effects on protein partitioning in size-exclusion chromatography and membrane ultrafiltration. *J. Chromatogr. A* **796,** 229–238 (1998).
13. Berg, H. C. *Random Walks in Biology* 34–37 (Princeton Univ. Press, Princeton, New Jersey, 1993).
14. Li, Q. Y., Cui, Z. F. & Pepper, D. S. Fractionation of HSA and IgG by gas sparged ultrafiltration. *J. Membr. Sci* **136,** 181–190 (1997).
15. Ku, J.-R. & Stroeve, P. Protein diffusion in charged nanotubes: ''On-off'' behavior of molecule transport. *Langmuir* **20,** 2030–2032 (2004).
16. Letant, S. E., Hart, B. R., Van Buuren, A. W. & Terminello, L. J. Functionalized silicon membranes for selective bio-organism capture. *Nature Mater.* **2,** 391–395 (2003).
17. Mace, C. R., Striemer, C. C. & Miller, B. L. Theoretical and experimental analysis of arrayed imaging reflectometry as a sensitive proteomics technique. *Anal. Chem.* **78,** 5578–5583 (2006).
18. Grom, G. F. *et al.* Ordering and self-organization in nanocrystalline silicon. *Nature* **407,** 358–361 (2000).
19. Reisman, A. *et al.* The controlled etching of silicon in catalyzed ethylenediamine-pyrocatechol-water solutions. *J. Electrochem. Soc.* **126,** 1406–1415 (1979).
20. Ouyang, H., Striemer, C. C. & Fauchet, P. M. Quantitative analysis of the sensitivity of porous silicon optical biosensors. *Appl. Phys. Lett.* **88,** 163108–163110 (2006).

Supplementary Information is linked to the online version of the paper at www.nature.com/nature.

Acknowledgements We thank R. Krishnan for assistance with ellipsometry and AFM, and for useful discussions; J. Snyder for assistance in preparing protein-treated membrane samples for TEM; B. McIntyre for assistance with microscopy; P. Osborne for help with equipment fabrication; and the Laboratory for Laser Energetics at the University of Rochester for providing access to their spectroscopic ellipsometer. Silicon microprocessing was conducted at the Hopeman Microfabrication Facility at the University of Rochester and the Semiconductor and Microsystems Fabrication Laboratory (SMFL) at the Rochester Institute of Technology. This work was partially supported by a Johnson & Johnson Award to the University of Rochester Medical School's Discovery Concept Fund.

Author Information Reprints and permissions information is available at www.nature.com/reprints. The authors declare no competing financial interests. Correspondence and requests for materials should be addressed to C.C.S. (striemer@ece.rochester.edu).

Supplementary Figures and Legends:

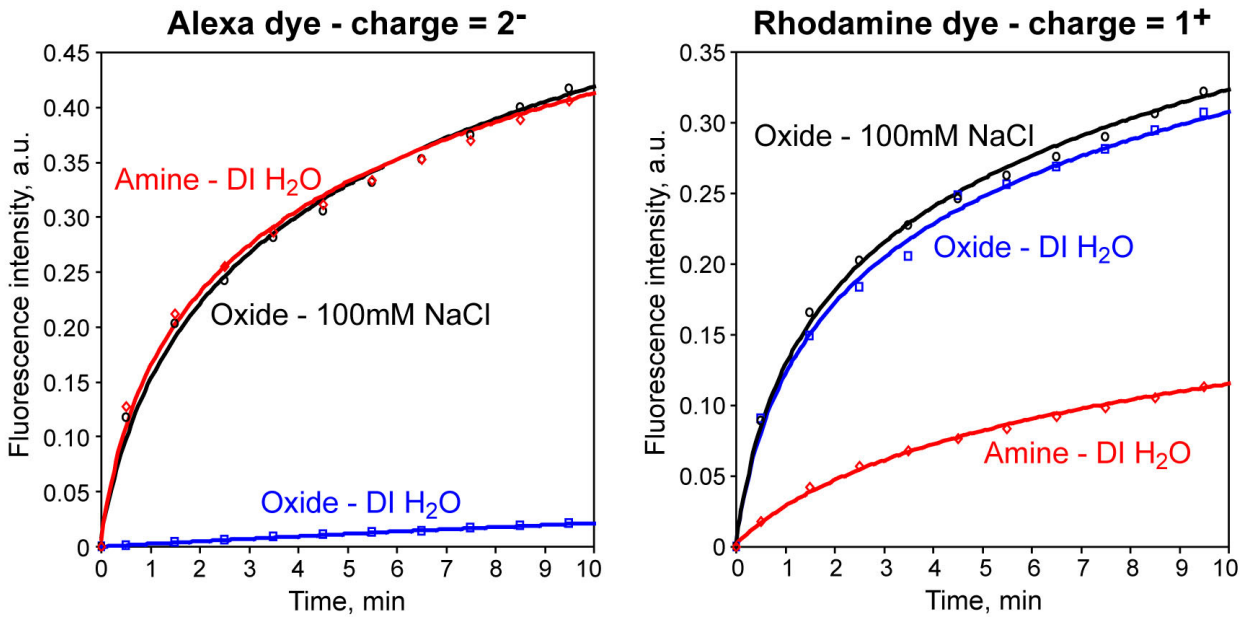

Supplementary Figure 1 Modulation of transport by surface modifications of Membrane A. An experiment was designed in which the transport rate of two types of dye with opposite charge (Alexa 488: charge=2- and rhodamine 6G: charge=1+) through membranes functionalized with opposite surface charge was studied. The first membrane treatment was simple oxidation (discussed in Methods), as SiO2 is known to carry a net negative surface charge at neutral pH. The second treatment involved covalent attachment of aminosilane to the membrane (see Methods), as amine groups are known to carry a net positive charge at neutral pH. Rhodamine 6G is slightly smaller than Alexa 488 (479 Da vs 885 Da), however the cutoff pore size of Membrane A is over 20x larger than either dye, making their relative size insignificant. It was found that Alexa 488 dye was transported efficiently through the amine-treated membrane at low ionic strength (0.05 mM dye in DI water), but was only transported through the oxidized membrane at high ionic strength (100 mM NaCl). Greater than 10x suppression of Alexa 488 transport through the oxidized membrane was observed at low ionic strength. For rhodamine 6G, the opposite effect was observed, efficient transport through the oxidized membrane for low and high ionic strength solutions, but ~3x suppression in transport through the amine-treated membrane. Therefore, molecular transport through pnc-Si membranes with like charge appears to be hindered by electrostatic repulsion and interaction with the electrochemical double (Debye) layer. These results not only demonstrate the importance of membrane and molecular charge in the transport through pnc-Si membranes, but show that this material can also be used to separate molecules based on their charge state.

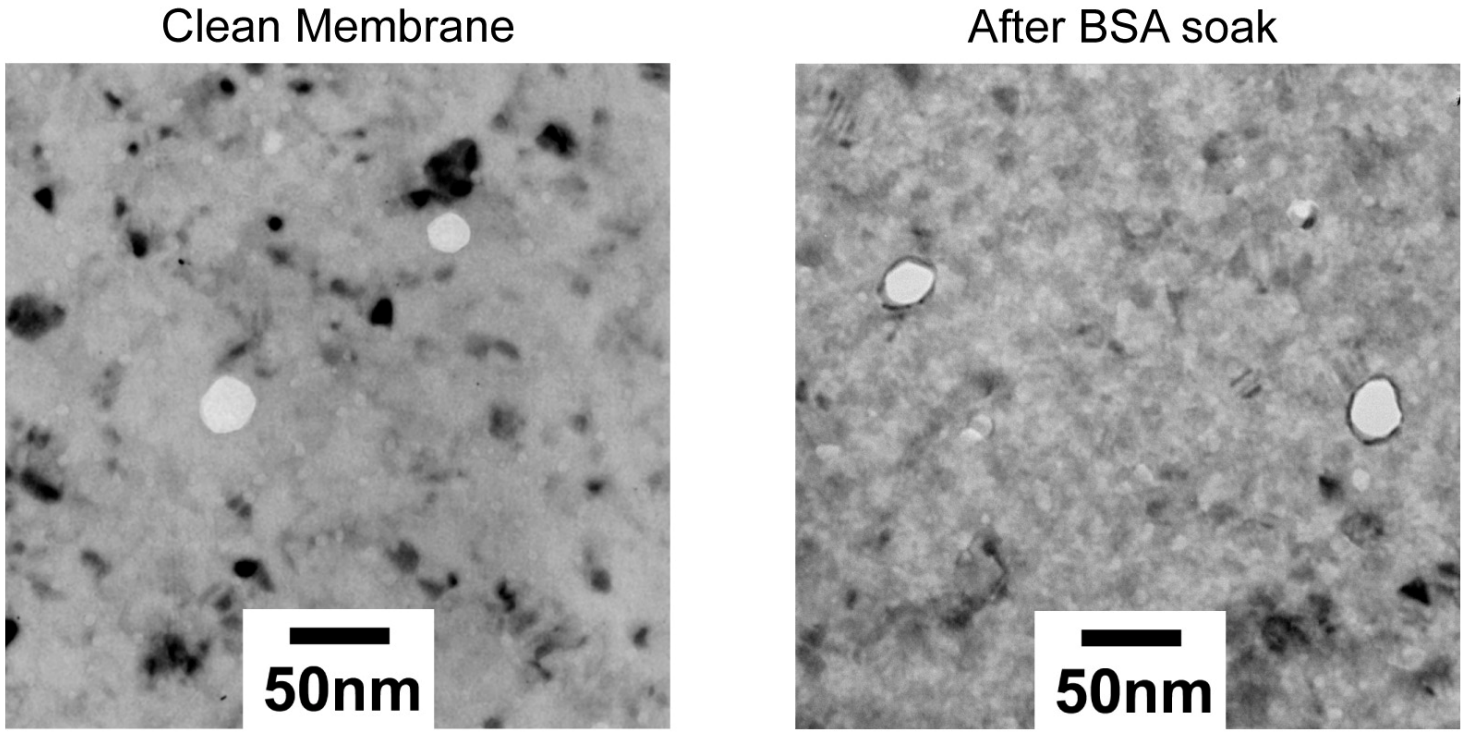

Supplementary Figure 2 Adsorption of protein changes the effective pore size of pnc-Si membranes. These two TEM images show a “clean” membrane that was never exposed to solution and another membrane after exposure to a 1 mg/mL BSA solution for 20 minutes. The membrane exposed to BSA was also stained with uranyl acetate (2% solution) to improve protein contrast in TEM imaging. Clean samples treated only with uranyl acetate showed no difference, confirming that any contrast enhancement is directly attributed to the protein. As shown in the images, exposure to BSA results in an observable dark protein ring, ~3.5 nm thick, within the pores. This size closely matches the approximate narrow dimension of the prolate-ellipsoid BSA molecule (14 nm x 3.8 nm x 3.8 nm)17 and likely indicates adsorption of a monolayer. The thickness of this coating does not increase over time, and therefore appears to be self-limiting. Such adsorption therefore tends to reduce the effective pore size by as much as 7 nm in separations involving BSA, without clogging the larger pores.

Supplementary Video Legend:

Supplementary Video 1 This time lapse movie shows the diffusion of free Alexa 546 dye and BSA through pnc-Si membrane A, as depicted in figure 4b. The movie shows the simultaneous transport of both species, one on each channel (488 nm or 546 nm) of a fluorescence microscope over 6.5 minutes of observation. The movie is in false color with high species concentration (red) initially in the region of the membrane, and diffusing over time into the area with no fluorescence (blue).

Supplementary Video 2 This time lapse movie shows the diffusion of BSA and IgG through pnc-Si membrane B, as depicted in figure 4c. The movie shows the simultaneous transport of both species, one on each channel (488 nm or 546 nm) of a fluorescence microscope over 6.5 minutes of observation. The movie is in false color with high species concentration (red) initially in the region of the membrane, and diffusing over time into the area with no fluorescence (blue).

9. Schuur, E. R. *et al. J. Biol. Chem.* **276,** 33554–33560 (2001).
10. Carroll, J. S. *et al. Cell* **122,** 33–43 (2005).
11. Wolf, I. *et al. Int. J. Cancer* **120,** 1013–1022 (2007).
12. Tong, Q. *et al. Science* **290,** 134–138 (2000).
13. Suh, J. M. *et al. Cell Metab.* **3,** 25–34 (2006).
14. Cantor, A. B. & Orkin, S. H. *Semin. Cell Dev. Biol.* **16,** 117–128 (2005).

NANOFLUIDICS

Silicon for the perfect membrane

Albert van den Berg and Matthias Wessling

Newly developed ultrathin silicon membranes can filter and separate molecules much more effectively than conventional polymer membranes. Many applications, of economic and medical significance, stand to benefit.

On page 749 of this issue, Striemer *et al.*[1] describe a method for preparing ultrathin nanoporous membranes made from silicon. Nanoporous membranes are already widely used in medicine, for instance for the filtration and separation of blood proteins in an artificial kidney (haemodialysis) — a rapidly growing world market currently worth more than US$1 billion annually. They can also function as a mechanical support for desalination membranes used to purify sea water for irrigation and human consumption. Given that the membrane technology is seemingly so mature, why should we bother searching for new methods and different starting materials?

At present, all technologically relevant nanoporous membranes are prepared by initiating the precipitation of a polymer from solution. This is achieved through the addition of a non-solvent (often water), or by rapid cooling. The solution precipitates into micrometre- and nanometre-sized domains rich in polymer that form a filter structure. Between these polymer domains, polymer-free areas form the pore system. A diverse spectrum of morphologies and geometries can thus be produced from a variety of starting materials[2].

These nanoporous membranes have a thin skin, typically less than 500 nanometres thick, made up of small bumps, or nodules, with a radius of a few to 50 nm. The voids between the nodules determine the pore size; the pores are 1–50 nm across, and thus the porosity of the membrane as a whole is low. A much thicker layer, with a larger pore size and porosity, provides mechanical support for the nodular skin. Although the pore size of the membrane skin can be adjusted by the choice of starting material and processing route, other morphological parameters, such as its thickness, porosity and pore-size distribution, are surprisingly insensitive to such choices[3].

Nanoporous membranes prepared according to these methods suffer from a typical trade-off: the flux through them can be enhanced by increasing the pore diameter, but at the cost of less effective molecular discrimination. Optimizing flux and selectivity simultaneously requires a fundamentally new approach, which Striemer and colleagues[1] offer.

Not only do the authors' porous nanocrystalline silicon (pncSi) membranes combine small membrane thickness and pore sizes (Fig. 1), but they are also robust, their pore size can be controlled, and they are simple to produce. Earlier attempts to make ultrathin nanoporous membranes used either sophisticated nanolithography or were based on colloidal templates[4,5]. The first method is expensive; and although the second makes elegant use of self-organization principles, very small, controlled pore sizes are difficult to achieve.

Striemer and colleagues' nanopores self-form from a deposited layer of amorphous silicon through rapid thermal annealing[6]. The pore sizes can be controlled between 5 and 25 nm (the range of interest for protein separation) by the choice of annealing temperature. Although the pore-size distribution is not extremely narrow, it has no tail to larger pore sizes. The absence of such a tail is a prerequisite for molecular specificity — and still a challenge for state-of-the-art polymer-based membranes.

The authors find that two important proteins, immunoglobulin-γ and bovine serum albumin (BSA), with hydrodynamic diameters of 14 and 6.8 nm, and molecular weights that similarly differ by a factor of a little more than two, can be separated using their pncSi membrane. For efficient separation using conventional ultrafiltration membranes, a molecular-weight ratio of more than ten is needed. The flux through the pncSi membranes is more than ten times faster than that through conventional membranes with similar selectivity properties. Moreover, Striemer *et al.*[1] find that by changing the surface charge of their membrane through chemical modification, they can separate proteins that are similar in size, but bear a different charge[7].

Perhaps the most promising advantage of the method presented by Striemer *et al.* is that it can be easily integrated into 'labs-on-a-chip' — microfluidics systems that are currently enjoying rapidly growing attention owing to their potential for medical diagnostics, drug discovery and chemical synthesis[8–10]. It is that promise of integration with other nanofluidic separation and analysis techniques for biochemical and biomedical applications that, together with the inherent advantages of the silicon-based system, make this such an important step forward. We look forward to further improvements and proposals for additional uses for the technique. ■

Albert van den Berg and Matthias Wessling are at the MESA+ Institute for Nanotechnology and the Faculty of Electrical Engineering, Computer Science and Mathematics, and the Faculty of Science and Technology, University of Twente, PO Box 217, Enschede, the Netherlands.
e-mail: a.vandenberg@utwente.nl

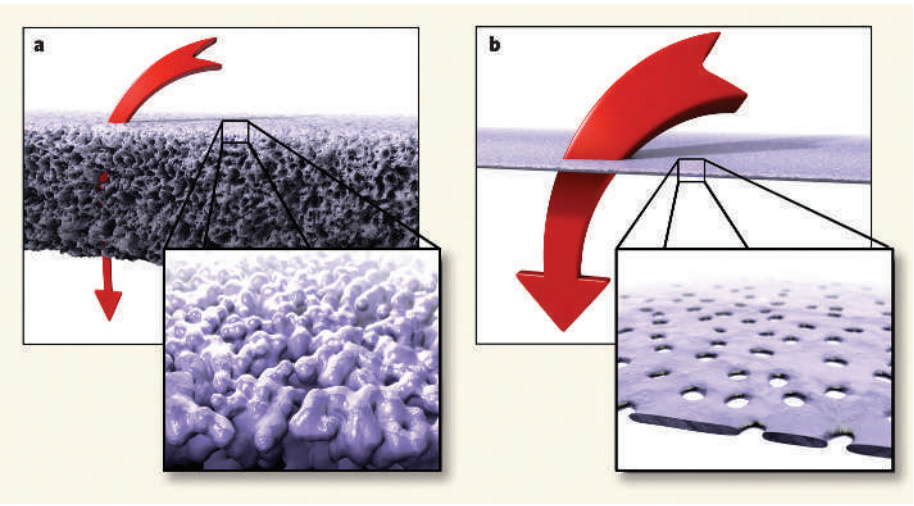

Figure 1 | Barrier to progress. a, The nanoscale nodules that make up the conventional ultrafiltration membrane form a significant restriction to flow. **b,** The ultrathin porous nanocrystalline silicon (pncSi) membranes developed by Striemer *et al.*[1] allow efficient protein separation without restricting the flow as much.

1. Striemer, C. C., Gaborski, T. R., McGrath, J. L. & Fauchet, P. M. *Nature* **445,** 749–753 (2007).
2. Vogelaar, L. *et al. Small* **1,** 645–655 (2005).
3. Mehta, A. & Zydney, A. L. *J. Membr. Sci.* **249,** 245–249 (2005).
4. Tong, H. D. *et al. Nano Lett.* **4,** 283–287 (2004).
5. Yan, F. & Goedel, W. A. *Adv. Mater.* **16,** 911–915 (2004).
6. Grom, G. F. *et al. Nature* **407,** 358–361 (2000).
7. Eijkel, J. C. T. & van den Berg, A. *Lab Chip* **6,** 19–23 (2006).
8. Whitesides, G. M. *Nature* **442,** 368–373 (2006).
9. van den Berg, A. & Bergveld, P. *Lab Chip* **6,** 1266–1273 (2006).
10. de Jong, J. *et al. Lab Chip* **6,** 1125–1139 (2006).

Research Highlights

Nature Nanotechnology Published online: 16 February 2007 | doi:10.1038/nnano.2007.60

Subject Category: Nanomaterials

Silicon: Filter to perfection

Ai Lin Chun

Abstract

New ultrathin silicon membranes can filter and separate molecules more efficiently than

conventional polymer membranes

Introduction

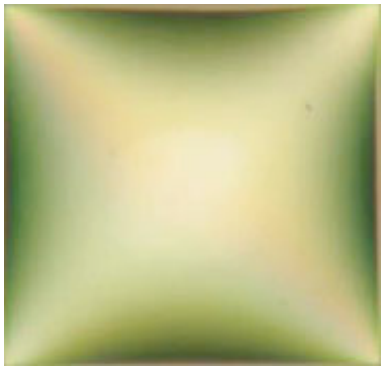

Commercial polymer membranes often have broad pore-size distributions that lead to poor separation and loss of material. Now, researchers at the University of Rochester in the USA have developed a new ultrathin porous nanocrystalline silicon membrane to overcome these problems in filtration and membrane separation technology.

By rapid thermal annealing of an amorphous layer of silicon, Christopher Striemer and colleagues[1] created a 10-nm-thick porous silicon membrane with pore sizes that can be easily controlled by changing the annealing temperature. When put to the test, this membrane could separate proteins of different sizes and molecular weights much faster than its polymer counterparts. Membranes that are chemically modified to have a different surface charge can also separate similar-sized proteins that bear different charges. Importantly, this new membrane is mechanically strong and easy to produce.

This new work is promising because it can be easily integrated into a microfluidics-based lab-on-a-chip system with potential medical diagnostic applications.

References

1. Striemer, C., Gaborski, T. R., McGrath, J. L. & Fauchet, P. M. Charge- and size-based separation of macromolecules using ultrathin silicon membranes. Nature 445, 749–753 (2007). | **Article** |

Top

Nature Nanotechnology

ISSN: 1748-3387

EISSN: 1748-3395

Banner image © Ward Lopes, Heinrich Jaeger